World Electric Vehicle Journal

MDPI

Article

Power Optimization of Multi-Type Mixed-Connection Photovoltaic Generation System for Recreational Vehicles

DaiBin Tang [1,2,*], Fei Lu Siaw [1] and Tzer Hwai Gilbert Thio [1]

[1] Centre for Sustainability in Advanced Electrical and Electronics Systems (CSAEES), Faculty of Engineering, Built Environment and Information Technology, SEGi University, Petaling Jaya 47810, Malaysia; siawfeilu@segi.edu.my (F.L.S.); gilbertthioth@segi.edu.my (T.H.G.T.)

[2] School of Electrical Engineering, Anhui Technical College of Mechanical and Electrical Engineering, Wuhu 241002, China

* Correspondence: sukd2101790@segi4u.my or ahjdtdb@ahcme.edu.cn

Abstract: The utilization of photovoltaic (PV) generation to charge storage batteries in recreational vehicles (RVs) is becoming increasingly prevalent. However, the performance of PV generation systems is hindered by the mismatch caused by different module types and varying environmental conditions. This discrepancy negatively impacts the output performance of PV modules, resulting in reduced system efficiency. To address this issue, this paper explored the series–parallel output characteristics of different types of PV modules and summarized the methods for configuring PV modules in a mixed-structure PV generation system for RV energy supplementation. Building upon this foundation, a novel equalization scheme based on extremum-seeking control (ESC) is introduced. The scheme initially employs a forward–flyback converter (FFC) to equalize the current among series-connected PV modules, followed by matching the voltage between parallel-connected PV module strings. Finally, the ESC is utilized to optimize the real-time output power of the PV generation system, thereby enhancing overall system efficiency. Through simulation experiments conducted on a PV generation system with four types of mixed-connection PV modules employing the PLECS simulation platform, simulated results demonstrate the effectiveness of the proposed scheme in improving PV module output performance and maximum power tracking efficiency. The simulation data reveal that the proposed scheme achieves an impressive average tracking efficiency of 99.15%, surpassing the efficiency of the global maximum power point tracking scheme based on an enhanced perturb and observe algorithm.

Keywords: photovoltaic modules; current equalization; voltage matching; extremum-seeking control; forward–flyback converter; PLECS

Citation: Tang, D.; Siaw, F.L.; Thio, T.H.G. Power Optimization of Multi-Type Mixed-Connection Photovoltaic Generation System for Recreational Vehicles. *World Electr. Veh. J.* **2024**, *15*, 125. https://doi.org/10.3390/wevj15040125

Academic Editor: Joeri Van Mierlo

Received: 22 February 2024
Revised: 17 March 2024
Accepted: 19 March 2024
Published: 22 March 2024

1. Introduction

Recreational vehicles (RVs) possess a distinct characteristic of mobility and serve as living spaces, necessitating reliable power sources. Typically, RVs are equipped with two types of batteries: a starting battery for vehicle power and a storage battery for daily living, as depicted in Figure 1a. Throughout history, supplementary energy storage for RVs has relied on various methods, including power generated during travel, charging from an external power grid, and power generated by onboard generators [1]. However, the advancement in solar cell efficiency, decreasing cost of PV panels, and environmentally friendly and noiseless nature of PV power generation have sparked interest in the use of solar power to supplement RV energy. This rising trend has garnered considerable attention and is widely recognized as an inevitable development in RVs. Typically, power generation systems in RVs employ a parallel connection structure, as illustrated in Figure 1b. However, due to limitations in roof installation conditions or the need for capacity upgrades, certain RVs integrate different types of PV modules. Consequently, mixed-connection systems have emerged, combining series–parallel connections of various PV module types, as shown

in Figure 1c. The performance disparities between different PV module types, as well as external factors like fallen leaves, shading from surrounding buildings, lamp posts, and trees, can lead to a decrease in the output performance of the PV modules. Moreover, these factors introduce complexity to the output power characteristics of the PV generation system. Traditional maximum power point tracking (MPPT) algorithms fail to accurately track the system's maximum power, thus adversely impacting the overall efficiency of the PV generation system.

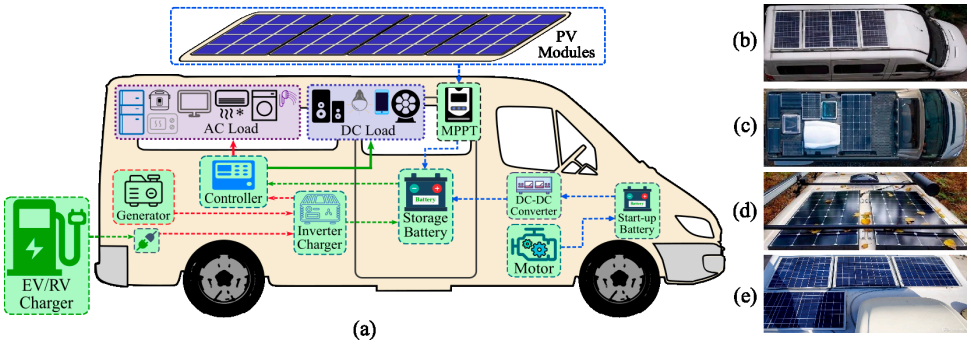

Figure 1. PV generation systems applied to RVs and different operating scenarios: (**a**) supplementation methods for RV storage batteries, (**b**) system consisting of the same type of PV modules, (**c**) system consisting of the different types of PV modules, (**d**) scenario of PV modules shaded by fallen leaves, and (**e**) scenario of partially shaded PV module.

In the practical implementation of PV generation systems, the initial design takes into account the consistency of PV module types to prevent mismatch issues caused by variations in PV module parameters [2]. The research and development of efficient and cost-effective solar cells for electric vehicles (EV) play a crucial role in the integrated development of PV generation technology and electric vehicle technology [3], and there has been significant research on modeling grid-connected EV–PV systems [4]. However, research specifically focused on PV generation systems applied to independent energy supply for RVs is extremely limited, with few related publications [5]. For the PV generation system depicted in Figure 1c, which comprises series–parallel connections of multiple types of PV modules, addressing mismatch issues caused by different PV module types is of paramount importance. This includes addressing current mismatches between PV modules in series, voltage mismatches between parallel connections, and mismatch issues arising from different environmental factors in order to enhance the output performance of each PV module. Additionally, the application of MPPT algorithms can improve the overall efficiency of the system.

In the existing research, the problem of mismatch in PV modules caused by environmental factors has been addressed through three types of power optimization schemes [6]. The first scheme is known as global maximum power point tracking (GMPPT) [7], which is suitable for PV generation systems with series-connected PV modules. However, this scheme is ineffective for PV generation systems with mixed connections, as each PV module string has its own global maximum power point (GMPP). The second scheme is the distributed maximum power point tracking (DMPPT) [8], which assigns a maximum power point tracker to each PV module to ensure maximum power output. However, this scheme has some drawbacks, including the requirement for multiple detection components and power devices, complex structure and control, and high cost. Moreover, the power converter used in the DMPPT scheme, known as the full power processor (FPP), processes the total power of all PV modules in the system, leading to power loss proportional to the processed power. This limitation hinders the overall efficiency improvement of the system [9]. The third scheme is the differential power processor (DPP) [10]. Compared to FPP, DPP only processes the power differences between series-connected PV modules, thereby reducing power loss and contributing to the overall efficiency enhancement of

the system. The application of DPP in PV generation systems can be categorized into three types: PV module–PV module (PV–PV), PV module–DC bus (PV–DC bus), and PV module–isolation port (PV–IP). In the PV–PV-based DPP structure, each DPP achieves power equalization between adjacent PV modules. However, for power balance between PV modules that are far apart, multiple power conversion processes need to be performed through intermediate DPPs, resulting in increased power loss, slower equalization speed, and lower efficiency [11]. In the PV–DC-bus-based DPP structure, energy equalization occurs directly between the PV modules and the DC bus, resulting in faster equalization speed and higher efficiency [12]. In the PV–IP-based DPP structure, electrical isolation is introduced between the PV modules and the isolated DC bus, thereby enhancing the safety of the system [13]. These two DPP structures commonly utilize bidirectional isolated DC converters, with flyback converters being the most frequently used [14,15]. However, the use of an isolated converter for each PV module in the system increases the overall cost. Furthermore, the necessity of detecting the voltage and current of the PV modules and controlling bidirectional energy flow adds complexity to the system structure and control.

PV generation systems consisting of multi-type PV modules with mixed connections face issues of current mismatch among series-connected PV modules and voltage mismatch between parallel-connected PV module strings. To enhance the output performance of each PV module, it is crucial to address both of these issues simultaneously. The single-switch multi-winding forward–flyback converter (FFC) can equalize the circuit for series-connected PV modules, while the multi-switch multi-winding forward–flyback converter can resolve the voltage mismatch problem for parallel-connected PV module strings. By considering the characteristics of both types of FFC, a proposed solution is the single-switch multi-transformer FFC, which can effectively tackle the mismatch problems in PV generation systems with mixed-connection PV modules, thereby improving the output performance of each PV module. Additionally, to achieve the maximum output power, it is necessary to incorporate the maximum power point tracking (MPPT) control technology. Traditional MPPT algorithms for PV generation systems, such as the incremental conductance algorithm [16] and the perturb and observe algorithm [17], primarily focus on controlling the power output of a single characteristic PV generation system. On the other hand, the GMPPT algorithm, like the enhanced perturb and observe (EPO) algorithm, is capable of performing segmented scanning on multi-peak characteristic PV generation systems to search for the GMPP of the system [18]. However, this algorithm necessitates many voltage- and current-sensing elements and microcontrollers and presents a complex circuit structure, leading to high costs. An alternative approach is extremum-seeking control (ESC), a nonlinear optimization technique that does not require detailed system knowledge [19]. ESC has been widely employed in various research fields, including industrial process control [20], source detection or localization [21], and energy conversion [22]. In one study [23], a sinusoidal ESC was implemented in a PV generation system using an analog circuit, resulting in oscillations near the maximum power point. Another study proposed a perturbation-based ESC algorithm, achieving efficiency up to 99.6% for GMPPT [24]. However, this algorithm necessitates multiple filtering and mean modules, as well as complex control parameter settings.

Following the Introduction, the subsequent section examines the performance characteristics of PV modules, as well as the output characteristics of multiple types of series–parallel connections of the PV modules, and provides a summary of the methods for configuring different types of PV modules in PV generation systems that are specifically designed for charging recreational vehicles. The third section delves into the operating principles of FFC used for current equalization and voltage matching and discusses their applications in different structures of PV generation systems. The fourth section introduces ESC algorithms, EPO algorithms, and maximum power converters. Moving forward, the fifth section conducts modeling and simulation of the equalization circuit and control algorithms using the power electronics system simulation platform PLECS. The sixth section discusses the simulation results. Finally, the last section summarizes this paper.

2. Characteristics of PV Modules and Methods for Configuring Multiple Types of PV Module Systems

2.1. Characteristics of Solar Cells and PV Modules

Solar cells, as shown in Figure 2a, which consist of semiconductor diode structures, serve as the fundamental unit of PV modules. Upon irradiation, carrier generation occurs at the p–n junction, resulting in the flow of current in a closed circuit [25]. The widely adopted theoretical and engineering approach employs the single-diode model, as depicted in Figure 2b. Multiple solar cells are interconnected in series or parallel and encapsulated into a PV module, as illustrated in Figure 2c. The *I*–*V* and *P*–*V* characteristic curves of a PV module are displayed in Figure 2d [26]. Incorporating parameters such as the equivalent series resistance R_s, the equivalent parallel resistance R_p, the series cell number N_s, and the parallel cell string count N_p, the *I*–*V* characteristic of a PV module can be described by Equation (1).

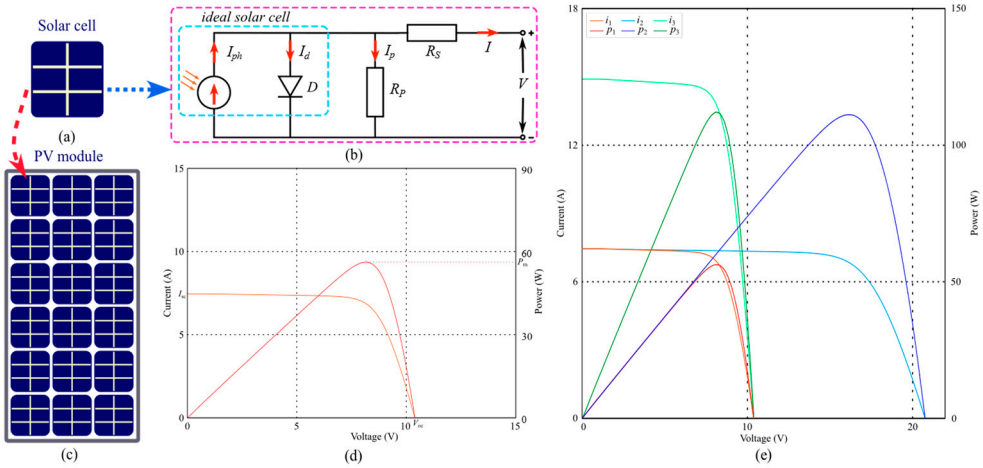

Figure 2. Solar cell and PV module: (**a**) solar cell, (**b**) single-diode model of solar cell, (**c**) PV module, (**d**) output characteristics of PV module, and (**e**) characteristics of series–parallel connection of the same type of PV modules.

$$I = I_{ph}N_p - I_0N_p\left[\exp\left(\frac{V + R_SI}{\alpha N_s kT/q}\right) - 1\right] - \frac{V + R_SI}{R_P} \quad (1)$$

where the variables represent the following:

I_{ph}: current generated by incident light;
I_0: reverse saturation or leakage current of diode;
q: electron charge ($1.60217646 \times 10^{-19}$ C);
k: Boltzmann constant ($1.3806503 \times 10^{-23}$ J/K);
T: temperature of the p–n junction (in Kelvin);
α: diode ideality constant.

In practical applications, the connection of PV modules in series or parallel is determined by specific voltage or power requirements. When PV modules are connected in series, the output current i_2 remains consistent with i_1, while the output voltage v_2 increases proportionally with the number of series-connected modules, as indicated by the blue curve in Figure 2e. Conversely, when PV modules are connected in parallel, the output voltage v_3 remains the same as v_1, while the output current i_3 is directly proportional to the number of parallel-connected modules, as demonstrated by the green curve in Figure 2e.

2.2. Output Characteristics of Different Types of PV Modules in Series or Parallel

When PV modules of different types are connected in series or parallel, the overall performance may decrease due to variations in their electrical characteristics [27]. To illustrate this, we will consider two types of monocrystalline silicon PV modules, referred

to as type-A (PV_1) and type-B (PV_2). Table 1 provides the key parameters of these PV modules, including open-circuit voltage V_{oc}, short-circuit current I_{sc}, and maximum power P_m under standard test conditions. From the table, it is evident that V_{oc1} is smaller than V_{oc2}, I_{sc1} is greater than I_{sc2}, and P_{m2} exceeds P_{m1}.

Table 1. Parameters of four different types of PV modules.

Type	A	B	C	D
N_s	18	24	36	66
V_{oc} (V)	10.4	14.6	21.90	41.4
I_{sc} (A)	7.5	5.41	5.14	5.55
P_m (W)	55.7	60.6	85.1	170
V_m (V)	8.1	11.95	17.72	33
I_m (A)	6.88	5.07	4.80	5.16

In the case of series-connected PV modules without a bypass diode (BD), the current under short-circuit conditions is represented as I_{sc2}, while the open-circuit voltage V_{oc} can be approximated as the sum of V_{oc1} and V_{oc2}. Additionally, the maximum power output P_{GM} is found to be less than the sum of P_{m1} and P_{m2}, as shown in Figure 3a. With the inclusion of a bypass diode, as depicted in Figure 3b, the output characteristics exhibit two distinct maximum power points, namely P_{LM} and P_{GM}, where P_{LM} slightly surpasses P_{m1}, and P_{GM} less than the sum of P_{m1} and P_{m2}.

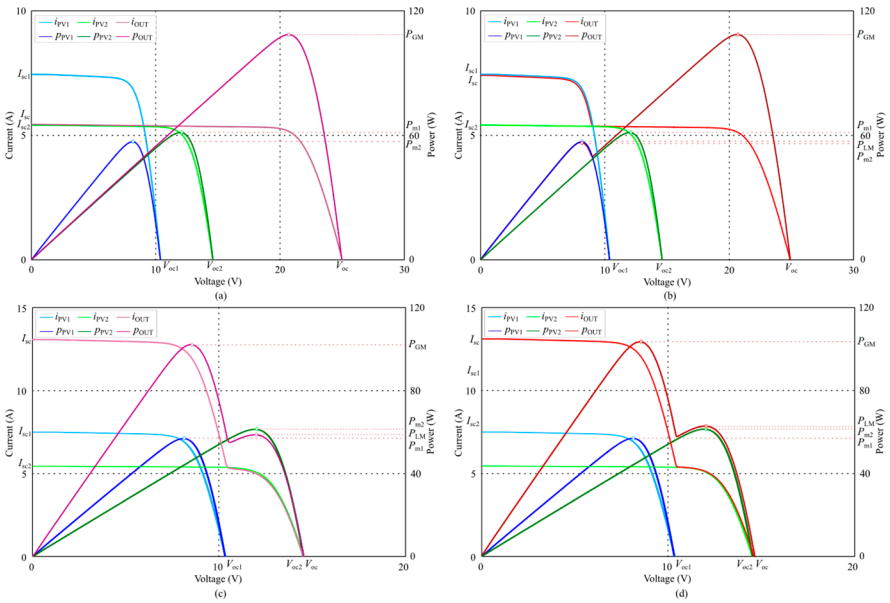

Figure 3. Characteristics of two types of PV modules: (**a**) connected in series without BD, (**b**) connected in series with BD, (**c**) connected in parallel without RD, and (**d**) connected in parallel with RD.

On the other hand, the output characteristics curve of parallel-connected PV modules presented in Figure 3c indicates that the open-circuit voltage V_{oc} is slightly smaller than V_{oc2} in the absence of a reverse diode (RD). When the output voltage is lower than V_{oc1}, the output current i_{OUT} is equal to the sum of i_{PV1} and i_{PV2}. However, when PV_1 reaches its maximum power, the parallel-connected PV modules exhibit a global maximum power P_{GM}, where P_{m1} is less than P_{GM}, and P_{GM} is less than the sum of P_{m1} and P_{m2}. When the operating voltage exceeds V_{oc1}, the output current i_{OUT} is lower than i_{PV2}, and when PV_2 reaches its maximum power, the output maximum power of the two PV modules is P_{LM}, which is less than P_{m2}. By introducing an RD, as displayed in Figure 3d, the output characteristics are modified. When the output voltage is lower than V_{oc1}, the global maximum power P_{GM} is the same, while the operating voltage exceeds V_{oc1}, the

output current i_{OUT} is equal to i_{PV2}, and when PV_2 reaches its maximum power, the output maximum power of the two modules is P_{LM}, approximately equal to P_{m2}.

By analyzing the data in Table 2 and referring to the curves in Figure 3, it becomes apparent that the BD has little effect on correcting the mismatch issue in series connections. Conversely, it leads to the appearance of two peaks in the *P*–*V* curve of interconnected PV modules. In the absence of protection provided by a BD, PV modules with a lower V_{oc} will transition from a power-generating state to an energy-consuming state, which may lead to damage during prolonged operation [28]. Similarly, an RD is used to prevent damage to PV modules with a lower V_{oc}, although it also results in a significant decrease in the output power of parallel-connected PV modules [29]. Considering the safety in engineering applications, PV modules should be equipped with a BD and an RD.

Table 2. Data of the output characteristics of two types of PV modules in series–parallel connection.

	Series Connection		Parallel Connection	
	Without BD	**With BD**	**Without RD**	**With RD**
V_{oc} (V)	24.98	24.98	14.50	14.59
I_{sc} (A)	5.44	7.46	12.85	12.85
P_m (W)	116.27	116.27	116.27	116.27
P_{GM} (W)	107.04	107.41	100.43	100.43
P_{LM} (W)	---	55.69	57.51	60.59

The *P*–*V* characteristic curves of three types (A, B, and C) and four types (A, B, C, and D) of PV modules connected in series or parallel with a BD or an RD are shown in Figure 4. Table 3 contains the relevant data for the characteristic curves shown in Figure 4. It is observed that the BD has a minor impact on the power output of series-connected PV modules, and the rate of mismatch loss changes minimally as the number of series-connected PV modules increases. On the other hand, the RD has a significant impact on the power output of parallel-connected PV modules, and the rate of mismatch loss increases correspondingly as the number of parallel-connected PV modules increases. Therefore, in practical engineering applications, series connections are often preferred.

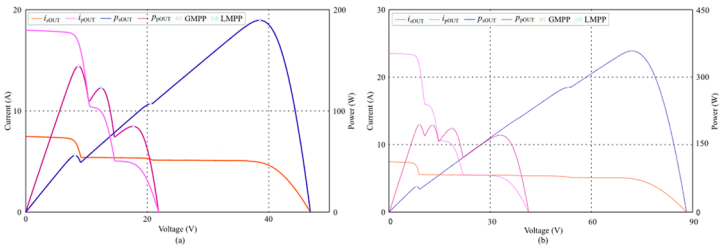

Figure 4. Characteristics of multiple types of PV modules in series or parallel connections: (**a**) three types of PV modules and (**b**) four types of PV modules.

Table 3. Data of the output characteristics of multiple types of PV modules in series (with BD) or parallel (with RD) connections.

	Three Types Connected in		Four Types Connected in	
	Series	**Parallel**	**Series**	**Parallel**
V_{oc} (V)	46.82	21.89	88.20	41.37
I_{sc} (A)	7.46	17.97	7.46	23.49
P_{RM} (W)	201.4	201.4	371.4	371.4
P_{GM} (W)	189.27	144.77	357.44	194.04
P_{LM1} (W)	55.69	122.99	55.69	192.95
P_{LM2} (W)	108.16	85.02	276.78	185.15
P_{LM3} (W)	---	---	---	170.05

In high-power situations, a mixed structure of series–parallel connection is often used to ensure the output voltage of a PV generation system meets the requirements for safe operation. Figure 5a depicts a mixed-connection PV generation system of eight type-A PV modules under non-uniform irradiance conditions, where the irradiance of PV_{21} and PV_{22} in PV $String_2$ is 200 W/m^2 and 600 W/m^2, respectively, while the irradiance of the remaining PV modules is 1000 W/m^2. Under this condition, the output characteristics of the PV generation system are shown in Figure 5b. It is evident that the series current and parallel voltage mismatch problems also exist in the mixed-connection PV generation system composed of the same type of PV modules.

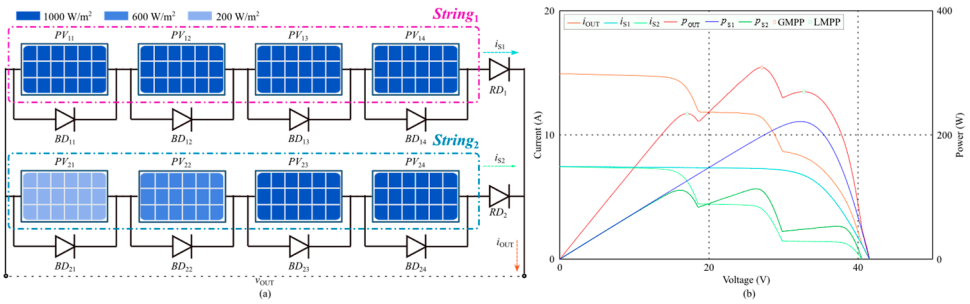

Figure 5. Mismatch of a PV generation system with the same type of PV modules under partial shading conditions: (**a**) system structure and (**b**) output characteristics.

2.3. Method of Configuring PV modules in Multi-Type Mixed Connection System

The analysis of the graphs and tabular data reveals the importance of carefully selecting appropriate PV modules and properly configuring them in a mixed-connection PV generation system [30]. This selection and configuration should be based on the power requirements and installation environment of the application, as well as the voltage of the storage battery or load. For instance, Figure 1c demonstrates a PV generation system in an RV that utilizes four types of PV modules. It is crucial to ensure the proper series–parallel configuration of these PV modules to maintain the efficiency of the PV generation system.

The data presented in Table 1 indicate the relationship between the open-circuit voltage V_{oc} of the PV module and the number N_s of solar cells connected in series within the PV module. Additionally, the short-circuit current I_{sc} is influenced by the type of solar cells utilized by the module manufacturer and the effective area of photoelectric conversion. When establishing a PV generation system, it is generally best to select PV modules of the same type. However, in the case of mixed series–parallel structure used for energy supplementation in recreational vehicles, the configuration of PV modules must also consider the voltage level of the vehicle's energy storage system. Recreational vehicle energy storage systems typically operate at voltage levels of 12 V, 24 V, and 48 V, with 12 V being the most common due to considerations of system structure rationality and electrical safety [31]. According to the standard that the maximum operating voltage V_m of the PV module should exceed 12 V, the last two types of PV modules listed in Table 1 can be configured in parallel. Conversely, PV modules with V_m lower than 12 V should be connected in series to meet charging requirements while ensuring that the output voltage after the series connection remains within the acceptable range for safety.

The combination of PV modules in a mixed series–parallel configuration needs to meet certain requirements based on circuit principles. These requirements include ensuring uniform short circuit current I_{sc} of PV modules connected in series and consistent open circuit voltage V_{oc} of PV modules or output voltage V_o of PV module strings in parallel connections. However, meeting these conditions in practical applications can be challenging. To address this issue, the proposed solution of this paper involves implementing a forward–flyback converter and its expanded structure to effectively resolve the mismatch issues encountered in the mixed series–parallel configuration of PV modules.

3. Forward–Flyback Converter-Based Equalizer

3.1. Current Equalization for Series-Connected PV Modules

Figure 6 depicts the proposed current equalizer utilized in the series connection of PV modules. This circuit combines both forward and flyback converters with a shared transformer, which serves to enhance efficiency. Through the parallel connection of their outputs, a consistent voltage output is attainable, concurrently diminishing the voltage pressure on the secondary rectifier. This approach leads to a more streamlined and effective design, particularly in cases where galvanic isolation is necessary. Although the primary winding configuration may be somewhat intricate, it facilitates the provision of multiple inputs as needed [32]. In the circuit, the primary winding W_1, capacitor C_4, and power switch devices S are shared. The forward converter, consisting of secondary windings W_3–W_5, excitation inductors Lm_1–Lm_3, and diodes D_4–D_6, is responsible for equalizing the current among the PV modules in series. On the other hand, the flyback converter, composed of secondary winding W_2, diode D_8, and capacitor C_5, facilitates power transmission to the load.

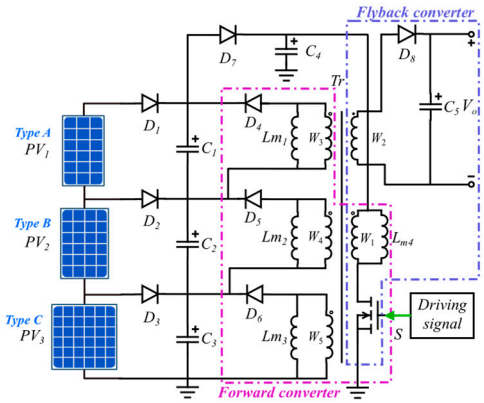

Figure 6. Proposed FFC-based current equalization applying to PV modules in series connection.

During each operation cycle of the converter, current equalization is performed during the forward mode [33]. Assuming that PV_1–PV_3 correspond to the A–C type PV modules in Table 1, and the three PV modules are operating at their maximum power points, meaning they are charging capacitors parallel with them at the maximum operating current, the voltages across capacitors C_1–C_3 are as follows:

$$V_{C1} = I_{m1} \cdot t / C_1 \tag{2}$$

$$V_{C2} = I_{m2} \cdot t / C_2 \tag{3}$$

$$V_{C3} = I_{m3} \cdot t / C_3 \tag{4}$$

Assuming that the capacitance value of capacitors C_1–C_3 is equal to C, the voltage across capacitor C_4 is determined as

$$V_{C4} = V_{C1} + V_{C2} + V_{C3} = (I_{m1} + I_{m2} + I_{m3}) \cdot t / C \tag{5}$$

After current equalization, the PV modules continue to operate at their maximum power points. Therefore, the output voltage of the secondary winding should match the maximum operating voltage of the connected PV module. Thus, the turns ratio between the primary winding W_1 and the secondary windings W_3–W_5 is calculated as

$$N_{W1} : N_{W3} : N_{W4} : N_{W5} = (V_{m1} + V_{m2} + V_{m3}) : V_{m1} : V_{m2} : V_{m3} \tag{6}$$

During the conduction period of the power switch S, the voltage V_{W1} on the primary winding is equal to the voltage V_{C4} across capacitor C_4. This allows the voltage on each equalization winding to be calculated as

$$V_{W3} = \frac{V_{m1}(I_{m1} + I_{m2} + I_{m3})}{V_{m1} + V_{m2} + V_{m3}} \cdot \frac{t}{C} \tag{7}$$

$$V_{W4} = \frac{V_{m2}(I_{m1} + I_{m2} + I_{m3})}{V_{m1} + V_{m2} + V_{m3}} \cdot \frac{t}{C} \tag{8}$$

$$V_{W5} = \frac{V_{m3}(I_{m1} + I_{m2} + I_{m3})}{V_{m1} + V_{m2} + V_{m3}} \cdot \frac{t}{C} \tag{9}$$

Based on the data presented in Table 1, the voltages across capacitors C_1–C_3 can be computed as 6.88 t/C, 5.07 t/C, and 4.80 t/C using Equations (2)–(4), respectively. Similarly, employing Equations (7)–(9), the voltages on the secondary windings W_3–W_5 are determined as 3.59 t/C, 5.30 t/C, and 7.86 t/C, respectively. Subsequently, the operation of the diodes in each equalization branch is as follows: D_1 is off, D_2 and D_3 are on, providing equalization energy to PV_2 and PV_3, while PV_1 transfers this equalization energy to the PV module string. When the output voltage of the equalization winding equals the voltage across the capacitor in parallel with it, the diode in that branch is turned off. The entire equalization process does not require voltage detection of each PV module, achieving automatic current equalization among them. Additionally, it allows the PV modules to operate near their maximum power points.

During the flyback mode, the power switch S is turned off, D_8 is on, and the stored energy in the transformer is released through the secondary winding W_2. Thus, energy transfer from the PV generation system to the load is achieved. Throughout this period, the current direction in the secondary winding W_2 is opposite to the current in the primary winding W_1 during the forward mode, eliminating the need for the reset winding of the magnetic core and simplifying the structure of the transformer.

3.2. Voltage Matching for Parallel-Connected PV Modules

The diagram in Figure 7 illustrates the circuit proposed for achieving voltage matching of parallel-connected PV modules. It utilizes a multi-switch, multi-winding forward–flyback converter. The primary side of the transformer windings W_1–W_3, power switches S_1–S_3, and excitation inductances Lm_1–Lm_3, which are shared for both the forward and flyback converters. On the secondary side, winding W_4 and inductance Lm_4 are dedicated to the flyback converter, responsible for output power and demagnetization. In the forward conversion stage, winding W_5 and diode D_5 play a critical role in ensuring voltage matching of parallel-connected PV modules.

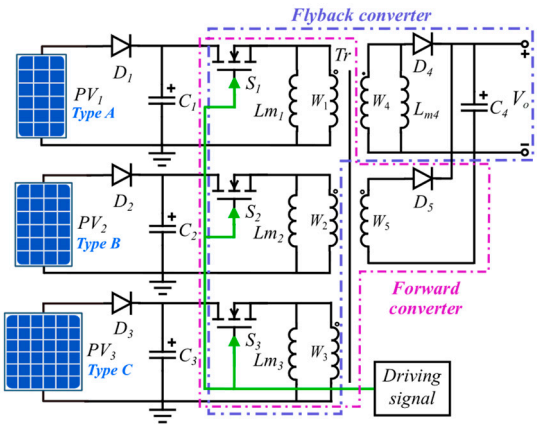

Figure 7. Proposed FFC-based voltage matching applying to PV modules in parallel connection.

The fundamental principle is based on voltage matching of the transformer. Therefore, the number of turns of each winding on the primary side is proportional to the maximum operating voltage of the connected PV module, while the number of turns of the two windings on the secondary side is equal to the maximum number of turns of the primary side winding. The specific calculation formula is given by Equation (10):

$$N_{W1} : N_{W2} : N_{W3} : N_{W4} : N_{W5} = V_{m1} : V_{m2} : V_{m3} : V_{\max} : V_{\max} \quad (10)$$

where $V_{\max}$ is the maximum of V_{m1}, V_{m2}, and V_{m3}.

3.3. Power Equalization for Mixed Series–Parallel-Connected PV Modules

By connecting the outputs of multiple current equalizers in parallel, it is possible to achieve current equalization and voltage matching in the PV generation system with mixed-connection PV modules. However, this configuration requires multiple power switches, leading to an increase in overall system cost and power loss. To address this issue, a new topology based on a single-switch, multi-transformer forward–flyback converter is proposed in this paper. The schematic diagram is illustrated in Figure 8.

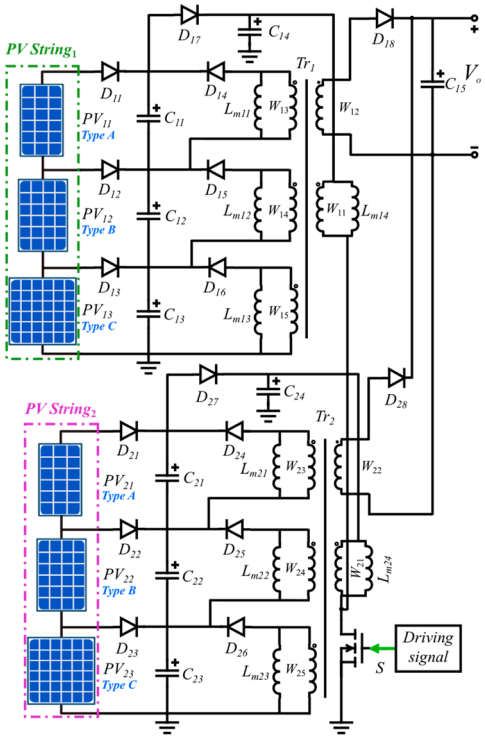

Figure 8. Proposed FFC-based power equalizer applying to PV modules in series–parallel connection.

The circuit mentioned above is an extension of the current-equalization concept proposed in Figure 6. It not only enhances the output performance of each series-connected PV module but also leverages the voltage-matching effect of the transformer. By appropriately setting the turns ratio of the transformer windings, each PV module can operate as close as possible to its maximum power point, thereby improving the overall output power of the PV generation system. The circuit utilizes the features of the PV–IP structure DPP by incorporating a transformer between the input and the output to ensure electrical isolation, thus improving system safety. Moreover, this configuration achieves automatic current equalization and voltage matching without requiring current and voltage detection components, utilizing only one power switch. This design simplifies the circuit layout compared to existing approaches, facilitating implementation and significantly reducing the system's economic costs.

4. Maximum Power Acquisition of PV Generation System Based on Extremum-Seeking Control

4.1. Extremum-Seeking Control

Figure 9a illustrates the approach for implementing MPPT using the sinusoidal ESC [23], which closely resembles the traditional perturbation and observation algorithm. In this approach, the perturbation signal γ is denoted as $\gamma = asin\ (\omega_0 t)$ and is introduced into the operating voltage of the PV generation system. In the detection block, a high-pass filter that isolates the AC power signal g from the output power multiplies the AC power signal g by the signal $K\gamma$ and extracts its DC component v using a low-pass filter, and then integrates v to obtain the perturbation direction signal Δu.

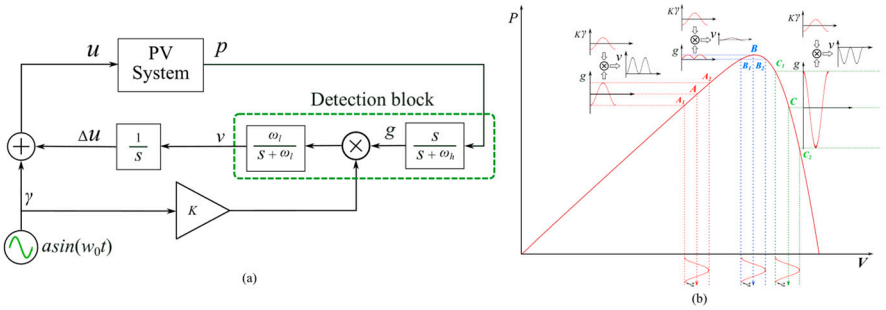

Figure 9. Sinusoidal ESC: (**a**) diagram of control block and (**b**) principle of ESC.

As depicted in Figure 9b, on the left side of the maximum power point, the phase of the AC power signal g extracted by the high-pass filter matches the signal $K\gamma$, resulting in both v and Δu being positive. This indicates that the perturbation direction is towards the right, thereby increasing the operating voltage of the PV generation system. Conversely, on the right side of the maximum power point, the phase of the AC power signal g is opposite to the signal $K\gamma$, and both v and Δu are negative. This signifies that the perturbation direction is towards the left, necessitating a decrease in the operating voltage of the PV generation system. Near the maximum power point, the frequency of g doubles, the change amplitude is small, v is positive or negative, and the integral value of v, Δu, approaches zero. Consequently, the operating voltage fluctuates near the maximum operating voltage of the PV generation system. The amplitude of the perturbation signal γ impacts the tracking accuracy, while the frequency ω_0 and proportional gain K impact the tracking speed. Excessive gain K may lead to system instability or oscillation near the maximum power point [34].

4.2. Maximum Power Converter

In the context of extremum-seeking control, the modification of the output voltage of the PV generation system necessitates the utilization of a DC–DC converter [35]. For this study, a buck converter is employed, and the traditional ESC control is improved to mitigate oscillations near the maximum power point. The specific approach is depicted in Figure 10. When the PV modules are shaded, or the irradiance changes dramatically, by detecting fluctuations in the output current i_{PV} of the PV generation system, integrating it, and obtaining the absolute value, the adjustment coefficient δ of the perturbation signal is generated. Consequently, during significant fluctuations in the output power of the PV generation system, the amplitude of the perturbation signal $\delta K\gamma$ increases accordingly. Conversely, near the maximum power point, the amplitude of the perturbation signal $\delta K\gamma$ decreases accordingly, thereby enhancing the tracking speed and reducing oscillations near the maximum power point. This is achieved by adjusting the duty cycle d of the driving signal of the power switch S in the buck converter to perturb the output voltage of the PV generation system.

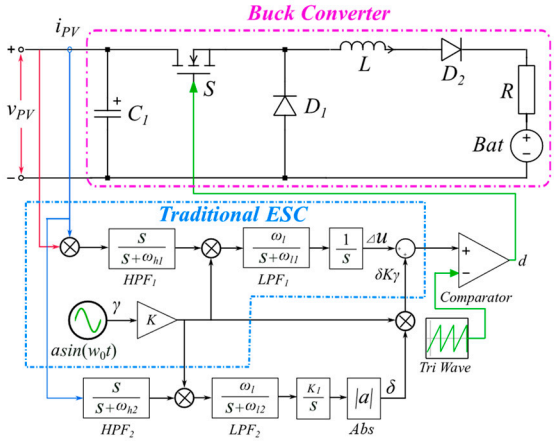

Figure 10. MPPT controller based on improved ESC and buck converter.

5. System Modeling and Simulation

To assess the efficiency of the proposed solution, we utilized the PLECS 4.7.7 software, tailored for power electronics and power transmission systems, to create simulation models and carry out simulations. PLECS provides an extensive selection of power components and control blocks, and its optimized solver allows for faster simulations compared to other similar software. Furthermore, it has a minimal storage requirement of approximately 750 MB, a user-friendly interface, a comprehensive waveform display, and robust data-processing capabilities, making it highly preferred by researchers [36].

5.1. System Modeling

This section specifically focuses on various models of the simulation, including the PV module block, equalization circuit, MPPT control, as well as signal acquisition, display, and data storage.

5.1.1. Modeling of PV Modules

Simulation models of four types of PV modules listed in Table 1 have been developed using PLECS [37]. These models are based on the single-diode model of the solar cell shown in Figure 2b and utilize the characteristic parameters provided in Table 1. Figure 11 displays the parameter setting interface for the simulation model corresponding to a type-A PV module, with the parameter settings for the other types of modules being similar to Figure 11.

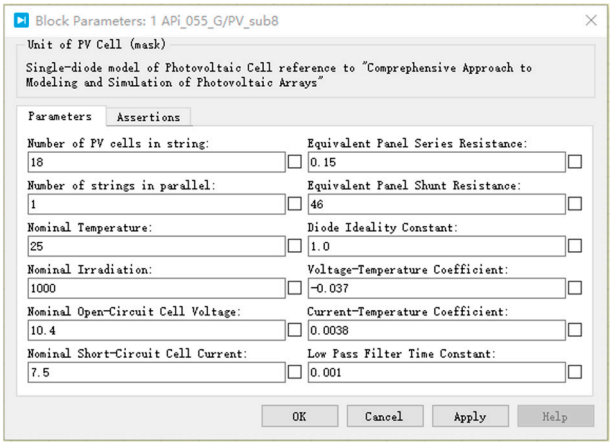

Figure 11. Block parameter setting interface for type-A PV module.

5.1.2. Modeling of Equalization Circuit

Figure 12 depicts the model of the current equalizer for series-connected PV modules. PV modules PV_1–PV_3 are linked to capacitors C_1–C_3 through reverse diodes D_1–D_3. The equalization branch is also connected to capacitors via diodes D_4–D_6. Power switch S is connected to capacitor C_4 through primary winding W_1. The output of the circuit comprises secondary windings W_2, diode D_8, and capacitor C_5. The temperature of each PV module is determined by a constant block T, and the irradiance is regulated using the 'From File' block, which will be elaborated upon in the simulation section.

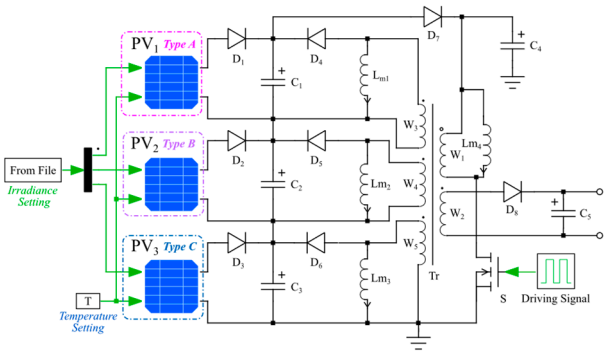

Figure 12. Simulation model of current equalizer for series connection of PV modules.

Figure 13 showcases the voltage-matching circuit for parallel-connected PV modules. The primary windings W_1–W_3 of the transformer are linked to capacitors C_1–C_3 through power switches S_1–S_3. The three PV modules are connected to capacitors C_1–C_3 through reverse diodes. The output comprises secondary windings W_4 and W_5 of the transformer, diodes D_4 and D_5, and capacitor C_4. The three PV modules are independent and connected in parallel through the transformer.

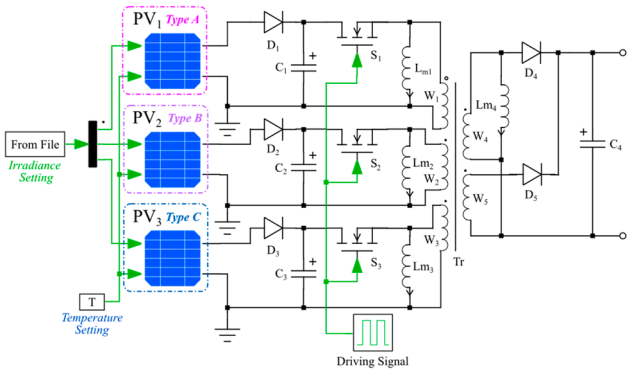

Figure 13. Simulation model of voltage-matching circuit for parallel connection of PV modules.

Figure 14 illustrates the power equalizer for a mixed connection of six PV modules. $String_1$ comprises two type-A PV modules and one type-B PV module. $String_2$ consists of two type-C PV modules, and $String_3$ solely contains one type-D PV module. The total maximum power of each PV module string is 170 W, and the total power of the PV generation system used for RV charging is 510 W. Each PV module string is equipped with a current equalizer, and the outputs of the three equalizers are connected in parallel.

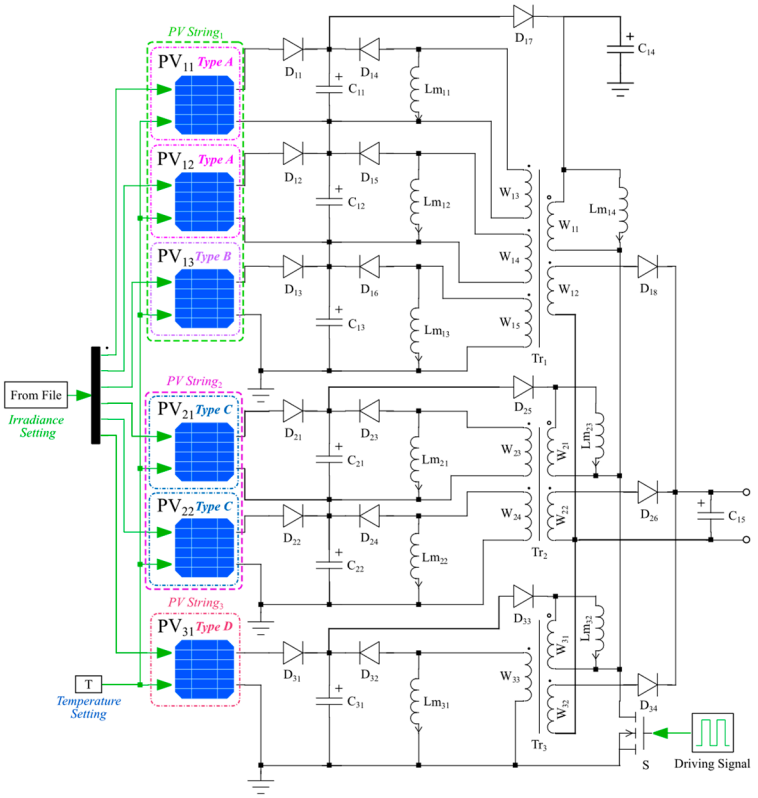

Figure 14. Simulation model of power equalizer for mixed connection of PV modules.

5.1.3. Modeling of ESC Algorithms and Maximum Power Converter

In Figure 15, the chart illustrates the MPPT control and power converter model utilized to achieve the maximum power of the PV generation system. The 'Probe' block plays a critical role in sensing the power, voltage, and current parameters of multiple devices or PV modules. Specifically, in Figure 15, the 'Probe' block is depicted detecting the voltage v_{PV} across capacitor C.

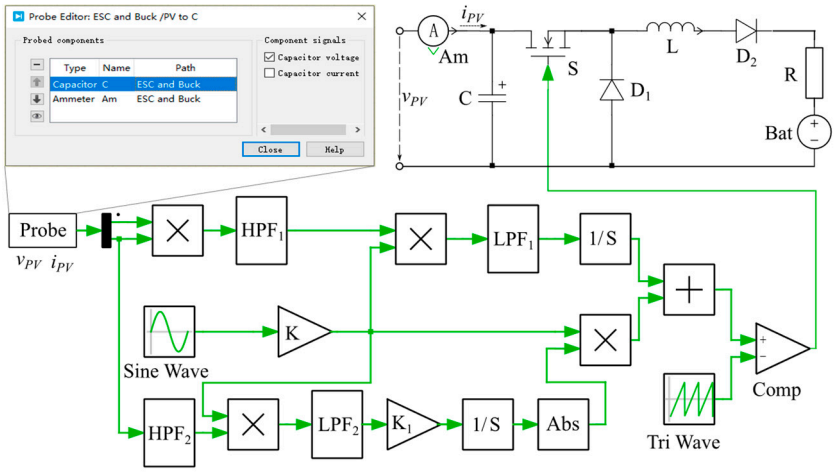

Figure 15. Simulation model of extremum-seeking control and buck converter applied to MPPT.

The simulation model of the GMPPT controller for the mixed-connection PV generation system based on the EPO algorithm proposed in the literature [18] is shown in Figure 16. The type, quantity, and irradiance of the PV modules in the figure are consistent with those in Figure 14. The fundamental principle of the EPO algorithm is to incorporate segmented scanning and global maximum power judgment functions based on the tradi-

tional perturbation and observation algorithm, enabling it to track the GMPP of the PV generation system under partial shading conditions. The 'Probe$_1$' block senses the output power of each PV module, then summed to derive the power p_{EPO} tracked based on the EPO algorithm.

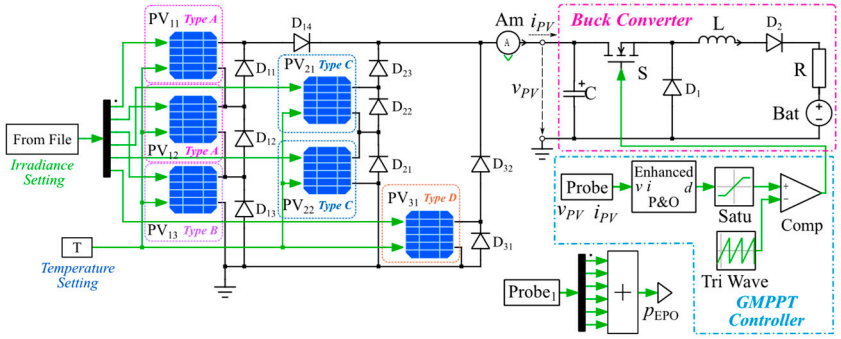

Figure 16. Simulation model of EPO algorithm and buck converter applied to GMPPT.

5.1.4. Modeling of Signal Sampling, Display, and Data Storage

Figure 17a illustrates the signal acquisition, display, and data storage model utilized in the simulation. As presented in Figure 17b, the 'Probe' block is employed to detect the voltage and power of PV_1–PV_3 in the current simulation model. These measured values are then summed to acquire the output voltage v_{PVs} and power p_{PVs} of the PV module string. The 'XY Plot' block is utilized to graph the P–V curve of the PV generation system, while the 'Scope' block is used to exhibit voltage curves, as well as power and current waveforms. Additionally, data obtained through the 'Probe' block can be stored in a comma-separated value file using the 'To File' block [38]. Figure 17c provides detailed instructions for the specific settings of the 'To File' block in the simulation, and the sampling time can be adjusted to achieve the desired accuracy.

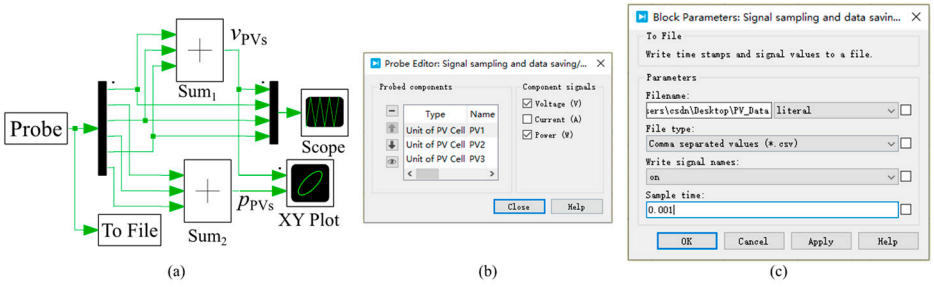

Figure 17. Simulation block for signal processing: (**a**) simulation block for signal acquisition, display, and data storage, (**b**) operating of 'Probe' block, and (**c**) setting of the 'To File' block.

5.2. Simulation Parameter Settings

5.2.1. Irradiance Settings

In the simulation model, the principal parameters of the PV modules are established based on the details presented in Table 1. The ambient temperature is standardized to 25 °C, representing standard test conditions. It is important to note that the performance of the PV modules is significantly impacted by the received irradiance. To define the required irradiance for the PV modules, the 'From File' block is utilized. Initially, a comma-separated value file is created to represent the changes in irradiance during the simulation. Subsequently, in the block parameter setting interface shown in Figure 18, the address and name of the file are entered under 'Filename' to establish a connection with the specified irradiance setting file. Furthermore, the number of output signals is determined, and the method of numerical variation for each time period is selected. By using the 'From File' module, the irradiance can be set to vary in a stepwise or linear manner.

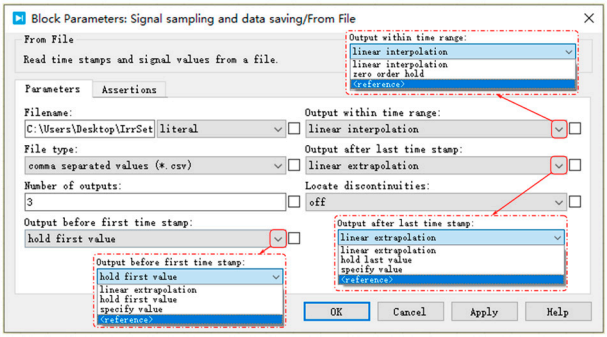

Figure 18. Simulation interface for PV module irradiance setting with 'From File' block.

It is important to note that the maximum power output of the PV module is directly proportional to the received irradiance. Therefore, the comma-separated value file can be used to specify the output maximum power P_M of the PV module under different irradiance levels. Additionally, it can also be utilized to determine the global maximum power P_{GM} of the PV generation system under different connection conditions. Throughout the simulation process, the instantaneous real maximum power p_{RM} and global maximum power p_{GM} values of the PV generation system can be obtained from this file, serving as references to calculate the maximum power tracking efficiency.

Table 4 presents the maximum power of each type of PV module at the corresponding irradiance levels, as well as the real maximum power and global maximum power of the PV generation system under three different connection modes.

Table 4. Maximum power of PV modules at different levels of irradiance and global maximum power of PV generation systems with various connection methods.

Power	Irradiance (W/m^2)				
	1000	**800**	**600**	**400**	**200**
P_{MA} (W)	55.70	44.86	33.67	22.27	10.81
P_{MB} (W)	60.57	48.59	36.40	24.08	11.75
P_{MC} (W)	85.02	68.25	51.15	33.84	16.50
P_{MD} (W)	170.02	136.63	102.45	67.78	32.99
$P_{MA} + P_{MB} + P_{MC}$ (W)	201.29	161.70	121.22	80.19	39.06
P_{GMS} (W)	189.27	151.72	113.39	74.46	35.33
P_{GMP} (W)	144.76	116.25	86.99	57.11	26.95
$2P_{MA} + P_{MB} + 2P_{MC} + P_{MD}$ (W)	512.03	411.44	308.49	204.08	99.36
P_{GMM} (W)	469.47	376.42	281.51	185.18	88.40

Note: P_{MA}–P_{MD} represents the maximum power of each type of PV module, P_{GMS} represents the global maximum power in series connection, P_{GMP} represents the global maximum power in parallel connection, and P_{GMM} represents the global maximum power in mixed connection.

5.2.2. Model Parameter Settings

It is noteworthy that the component parameters in the simulated models of different equalization circuits, buck converters, and control blocks proposed in this study are fundamentally identical. The specific settings for these parameters can be found in Table 5.

Table 5. Parameters of components in the simulation model.

Model	Type	Name	Value	Unit
Series/ Parallel Connection	Capacitor	C_1, C_2, C_3	0.1	F
	Capacitor	C_4, C_5	1000	μF
	Inductor	Lm_1, Lm_2, Lm_3	10	μH
	Inductor	Lm_4	2.2	mH
	Transformer	N_{W1}:N_W:$_2N_{W3}$:N_{W4}:N_{W5} (Series)	38:−38:8:12:18	---
	Transformer	N_{W1}:N_{W2}:N_{W3}:N_{W4}:N_{W5} (Parallel)	8:12:18:−18:18	---

Table 5. *Cont.*

Model	Type	Name	Value	Unit
Mixed Connection	Capacitor	C_{11}, C_{12}, C_{13}	0.1	F
	Capacitor	C_{21}, C_{22}	0.066	F
	Capacitor	C_{31}	0.033	F
	Capacitor	C_{14}, C_{15}	1000	μF
	Inductor	Lm_{11}, Lm_{12}, Lm_{13}, Lm_{21}, Lm_{22}, Lm_{31}	100	μH
	Inductor	Lm_{14}	2.2	mH
	Inductor	Lm_{23}	3.3	mH
	Inductor	m_{32}	2.7	mH
	Transformer	N_{W11}:N_{W12}:N_{W13}:N_{W14}:N_{W15} (Tr_1)	113:−142:32:32:49	---
	Transformer	N_{W21}:N_{W22}:N_{W23}:N_{W24} (Tr_2)	142:−142:71:71	---
	Transformer	N_{W31}:N_{W32}:N_{W33} (Tr_3)	134:−142:134	
Buck Converter	Inductor	L	0.2	mH
	Resistor	R	0.01	Ω
	Battery	V_{Bat}	12	V
	Driving	f	100	KkHz
	Signal	D	0.48	---
ESC Controller	HPF_1, HPF_2	τ	0.01	s
	LPF_1, LPF_2	τ	0.02	s
	Gain	K/K_1	50/40,000	---
	Sine Wave	a/f	0.0005/50	V/Hz
	Tri Wave	f	50	kHz
GMPPT Controller	Satu	Upper limit/Lower limit	0.5/0.32	---
	Tri Wave	f	50	kHz

5.3. Simulation of Series/Parallel-Connected PV Generation System

The simulation can be categorized into two situations, uniform irradiance (0–12 s) and non-uniform irradiance (12–22 s), as illustrated in Table 6, each of which can be further classified into step changes and linear changes. Table 6 provides the values for the irradiance settings during the simulation period, as well as the real maximum power P_{RM} and global maximum power P_{GM} of the PV generation system at each corresponding irradiance level.

Table 6. Irradiance of each PV module, real maximum power, and global maximum power of the PV generation system in series or parallel connection.

Scenarios	Change Mode	Time (s)	G_1 (W/m^2)	G_2 (W/m^2)	G_3 (W/m^2)	P_{RM} (W)	P_{GMS} (W)	P_{GMP} (W)
Uniform Irradiance	Step	0–1	1000	1000	1000	201.29	189.27	144.76
		1–2	800	800	800	161.70	151.72	116.25
		2–3	600	600	600	121.22	113.39	86.99
		3–4	400	400	400	80.19	74.46	57.11
		4–5	200	200	200	39.06	35.33	26.95
		5–6	600	600	600	121.22	113.39	86.99
		6–7	1000	1000	1000	201.29	189.27	144.76
	Linear	8	800	800	800	161.70	151.72	116.25
		9	600	600	600	121.22	113.39	86.99
		10	400	400	400	80.19	74.46	57.11
		11	200	200	200	39.06	35.33	26.95
		12	1000	1000	1000	201.29	189.27	144.76
Non-Uniform Irradiance	Step	12–13	1000	1000	800	184.52	156.14	135.74
		13–14	1000	1000	600	167.42	118.92	126.77
		14–15	1000	1000	400	150.11	107.04	117.84
		15–16	1000	1000	200	132.77	107.04	109.00
		16–17	1000	800	400	138.13	87.02	108.51
		17–18	1000	600	200	108.60	65.86	90.54
		18–19	1000	400	200	96.28	55.69	81.44
	Linear	20	1000	600	400	125.94	78.44	99.28
		21	1000	800	600	155.44	117.90	117.35
		22	1000	1000	800	184.52	156.14	135.74

5.3.1. Simulation of Series-Connected PV Generation System

The simulation results of the series-connected PV generation system are illustrated in Figure 19.

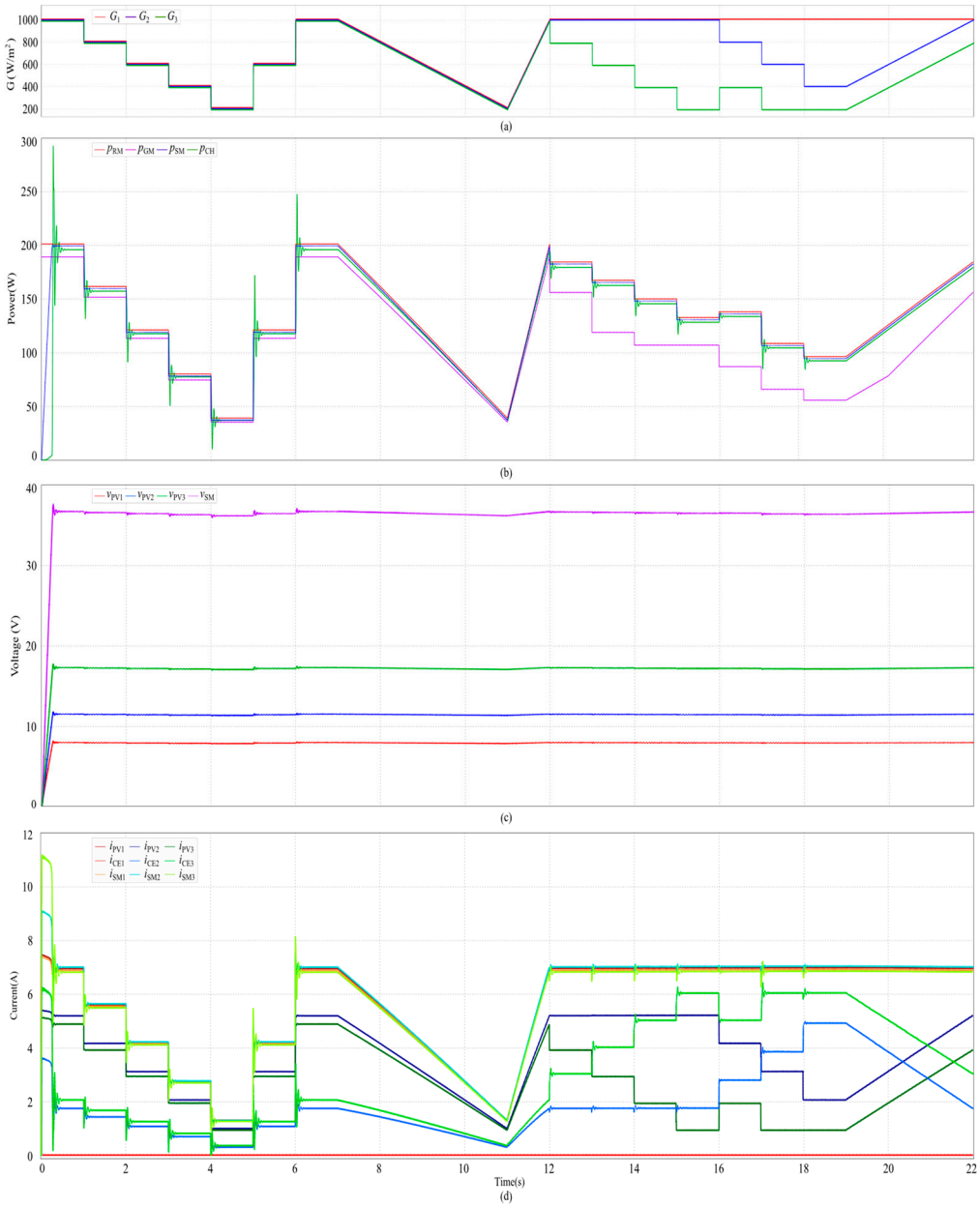

Figure 19. Simulated waveforms of series-connected PV system: (**a**) irradiance of each PV module and the various (**b**) powers, (**c**) voltages, and (**d**) currents.

Figure 19a depicts the changes in irradiance over the simulation period. Meanwhile, Figure 19b displays the simulated waveforms of the various powers of the PV generation system. The p_{RM} represents the sum of the instantaneous real maximum power of each PV module under different irradiance levels, as specified in Table 6, signifying the real-time maximum power output of the PV generation system. On the other hand, p_{GM} denotes the instantaneous global maximum power of the PV generation system, showing linear proportional changes with irradiance. Additionally, p_{SM} showcases the instantaneous maximum power output of the series-connected PV modules using current-equalization technology, while p_{CH} represents the instantaneous power of battery charging detected by the 'Probe' block. Analysis of the graphs reveals that p_{SM} is slightly smaller than p_{RM} but

significantly greater than p_{GM}. Moreover, p_{CH} exhibits oscillations in response to sudden changes in irradiance but stabilizes quickly, with the stabilized p_{CH} surpassing p_{GM}.

Figure 19c presents the waveforms of the output voltage of each PV module and the PV module string in the series-connected PV generation system. It is evident that, after stabilization, the output voltage of each PV module is maintained at the maximum operating voltage, ensuring the overall stability of the PV generation system's output voltage.

Figure 19d depicts the simulated waveforms of the output current, equalization current, and equalized current of each PV module in the series-connected PV generation system. Here, i_{PV1}, i_{PV2}, and i_{PV3} represent the output currents of PV_1, PV_2, and PV_3, respectively. Correspondingly, i_{CE1}, i_{CE2}, and i_{CE3} represent the equalization currents of the PV modules. Additionally, i_{SM1}, i_{SM2}, and i_{SM3} represent the sum of the output current and equalization current of each PV module, known as the equalized current of the PV module. The value of i_{CE1} is consistently zero, indicating no equalization current on PV_1, and the diode D_4 on the corresponding equalization branch is always in the off-state. Conversely, the values of i_{CE2} and i_{CE3} also vary with changes in irradiance. Importantly, when the system stabilizes, the values of i_{SM1}, i_{SM2}, and i_{SM3} are equal, achieving current equalization among the series-connected PV modules. The simulated waveforms offer empirical evidence supporting the principle of current equalization mentioned above.

Figure 20 illustrates the trajectories of the maximum power point of each PV module and the series-connected PV generation system. The figure demonstrates the stability of the maximum operating voltage of each PV module, with minor fluctuations occurring during sudden irradiance changes. This emphasizes the effectiveness of the current equalizer in achieving current equalization within the PV module string and ensuring each PV module operates at its maximum power point, thereby stabilizing the output voltage.

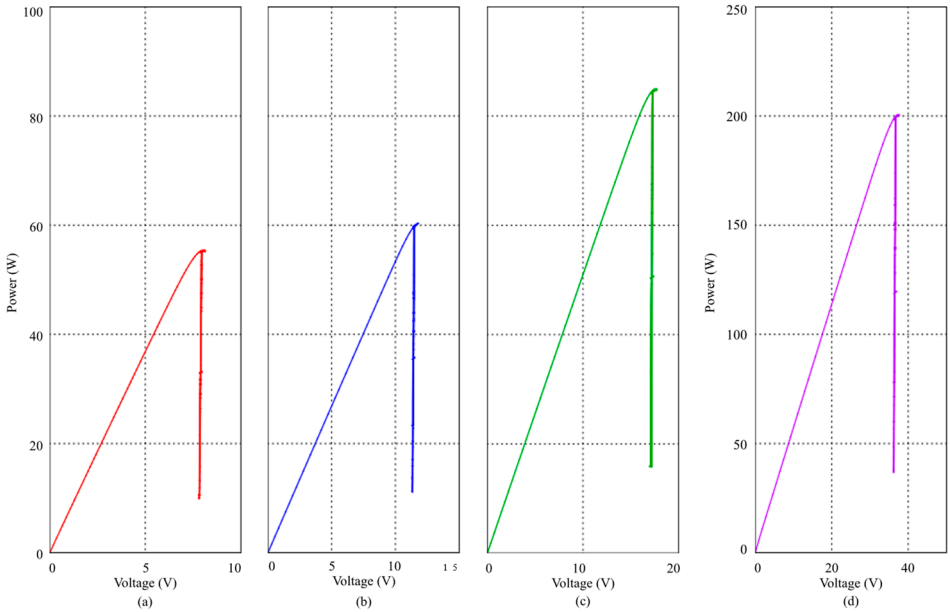

Figure 20. MPP trajectories of (**a**) PV_1, (**b**) PV_2, (**c**) PV_3, and (**d**) series-connected PV generation system.

5.3.2. Simulation of Parallel-Connected PV Generation System

The simulation results of the parallel-connected PV generation system are presented in Figure 21. Figure 21a shows that the p_{SM} and p_{CH} are slightly smaller than p_{RM}, while the p_{GM} is significantly smaller than these values. This highlights the crucial role of the voltage-matching circuit in enhancing the output performance of PV modules and the overall system efficiency. The waveforms of the output voltage of each PV module, as depicted in Figure 21b, further support this observation, where after stabilization, the output voltage of each PV module stabilizes at its maximum operating voltage.

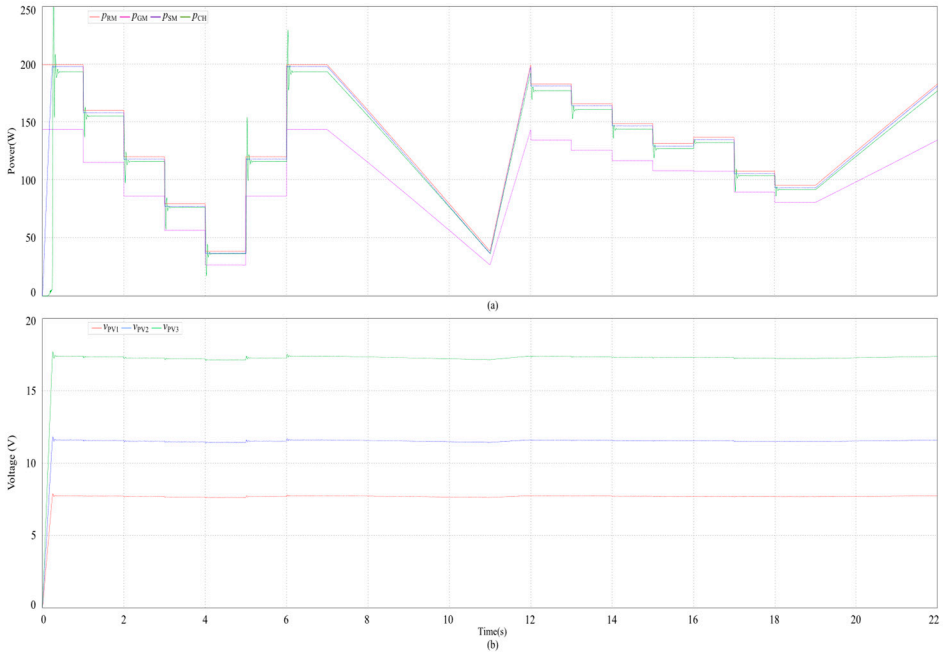

Figure 21. Simulated waveforms of parallel-connected PV power system: (**a**) various powers and (**b**) voltages of each PV module.

Figure 22 illustrates the trajectories of the maximum power point of each PV module in the parallel-connected PV generation system. Once the system stabilizes, each parallel-connected PV module operates at the maximum power point, maintaining a consistent maximum operating voltage despite significant variations in irradiance.

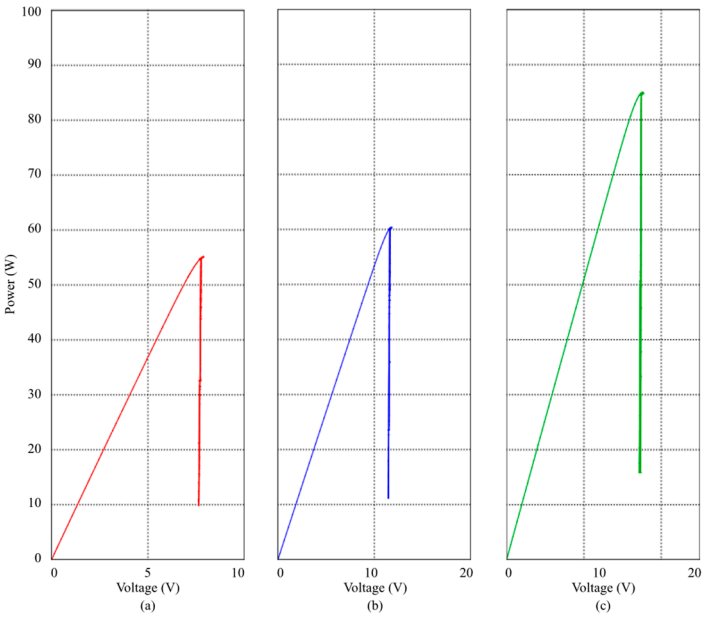

Figure 22. MPP trajectories of parallel-connected PV power system: (**a**) PV_1, (**b**) PV_2, and (**c**) PV_3.

5.4. Simulation of Mixed-Connection PV Generation System

Table 7 provides the irradiance of each PV module in a mixed-connection PV generation system, along with real maximum power P_{RM} and global maximum power and P_{GM}.

Table 7. Irradiance of each PV module, real maximum power, and global maximum power of the PV generation system in mixed connection.

Scenarios	Change Mode	Time (s)	G_{11} (W/m^2)	G_{12} (W/m^2)	G_{13} (W/m^2)	G_{21} (W/m^2)	G_{22} (W/m^2)	G_{31} (W/m^2)	P_{RM} (W)	P_{GM} (W)
Uniform Irradiance	Step	0–1	1000	1000	1000	1000	1000	1000	512.03	469.47
		1–2	800	800	800	800	800	800	411.44	376.42
		2–3	600	600	600	600	600	600	308.49	281.51
		3–4	400	400	400	400	400	400	204.08	185.18
		4–5	200	200	200	200	200	200	99.36	88.40
		5–6	600	600	600	600	600	600	308.49	281.51
		6–7	1000	1000	1000	1000	1000	1000	512.03	469.47
	Linear	8	800	800	800	800	800	800	411.44	376.42
		9	600	600	600	600	600	600	308.49	281.51
		10	400	400	400	400	400	400	204.08	185.18
		11	200	200	200	200	200	200	99.36	88.40
		12	1000	1000	1000	1000	1000	1000	512.03	469.47
Non-Uniform Irradiance	Step	12–13	800	1000	1000	1000	800	1000	484.42	433.17
		13–14	600	1000	1000	1000	600	1000	456.13	383.10
		14–15	400	1000	1000	1000	400	1000	427.42	316.84
		15–16	200	1000	1000	1000	200	1000	398.62	286.10
		16–17	800	1000	400	800	400	800	363.36	262.22
		17–18	600	1000	200	600	200	600	271.22	181.29
		18–19	400	1000	200	400	200	400	207.84	128.52
	Linear	20	600	1000	400	600	400	600	300.89	227.02
		21	800	1000	600	800	600	800	392.99	323.20
		22	1000	1000	800	1000	800	1000	483.28	416.39

Figure 23 depicts the simulated waveforms of the mixed-connection PV generation system. Figure 23a shows the irradiance variation curves during the simulation period, while Figure 23b displays the waveforms of various powers. The instantaneous maximum power p_{SM} tracked by the proposed scheme is slightly lower than the instantaneous real maximum power p_{RM}. Although the instantaneous charging power p_{CH} of the battery is lower than that of p_{SM} and p_{RM}, it still remains higher than the instantaneous global maximum power p_{GM} and the instantaneous maximum power p_{EPO} tracked by the EPO algorithm. Additionally, p_{EPO} exhibits oscillations throughout the process, particularly during sudden changes in irradiance.

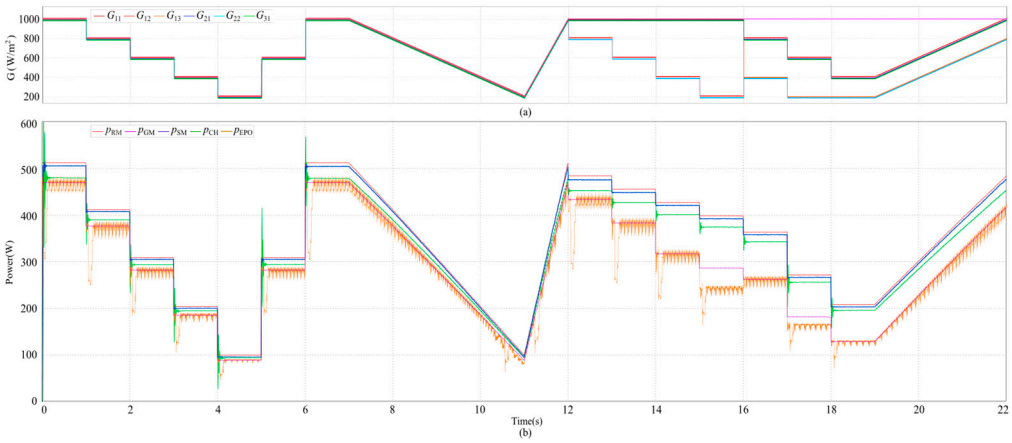

Figure 23. Simulated waveforms of mixed-connection PV generation system: (**a**) irradiance of each PV module and (**b**) various powers.

Figure 24a showcases the voltage waveforms, indicating that the PV module strings in the PV generation system, using equalization technology, as well as each PV module within the PV module string, operate at the maximum operating voltage and vary accordingly with changes in irradiance. Meanwhile, Figure 24b presents the voltage waveforms of each PV module based on the EPO algorithm, showing different degrees of fluctuations, with the magnitude of the fluctuations related to the maximum operating voltage of the PV modules and the changes in received irradiance. This suggests that the EPO-based algorithm is constantly regulating the operating voltage of each PV module in the PV generation system, particularly during sudden changes in irradiance, with a significantly increased magnitude of regulation.

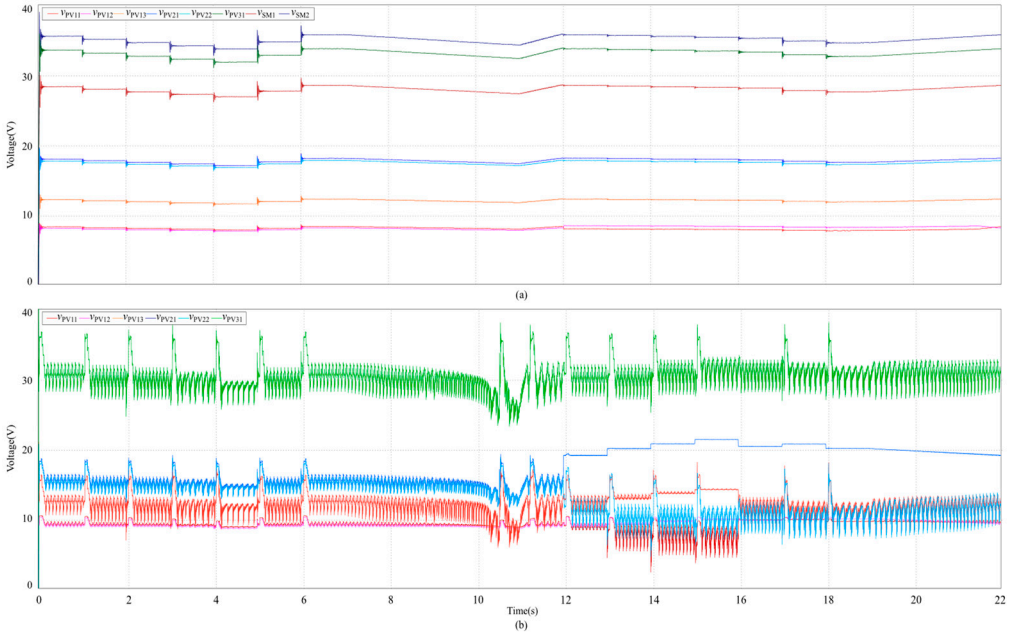

Figure 24. Simulated voltage waveforms of mixed-connection PV generation system: (**a**) proposed scheme and (**b**) EPO-algorithm-based GMPPT scheme.

Figure 25 depicts the simulated waveforms of the output current, equalization current, and equalized current of each PV module in $String_1$ of the mixed-connection PV generation system. The equalization effect mirrors that of Figure 19d, except for the equalization current i_{CE12}, which is consistently zero, signifying the absence of equalization current on PV_{12}, and the corresponding diode D_{15} on the equalization branch remains in the off-state. In contrast, the values of i_{CE11} and i_{CE13} change correspondingly with variations in irradiance.

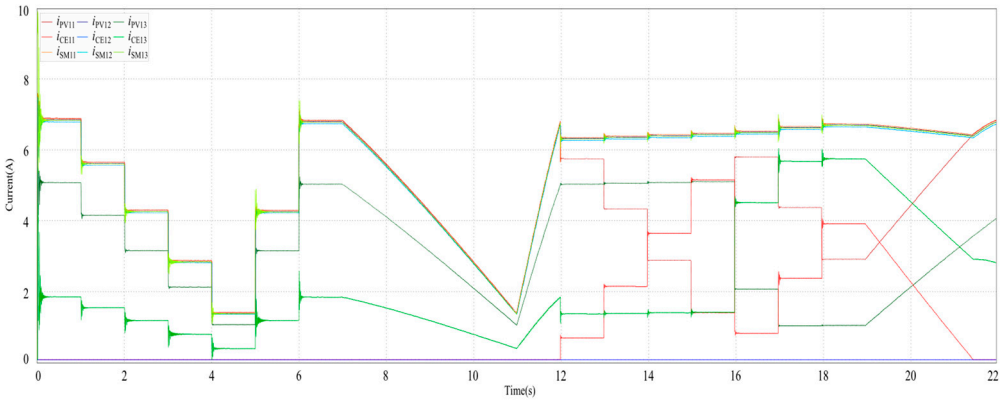

Figure 25. Simulated current waveforms of mixed-connection PV generation system.

Figure 26 illustrates the detailed trajectories of the maximum power points of each PV module or PV module string in the mixed-connection PV generation system using the proposed scheme. At the initial stage of the system startup, the maximum power point undergoes several oscillations before stabilizing. There is a slight oscillation during sudden changes in irradiance, while the rest of the time remains relatively stable.

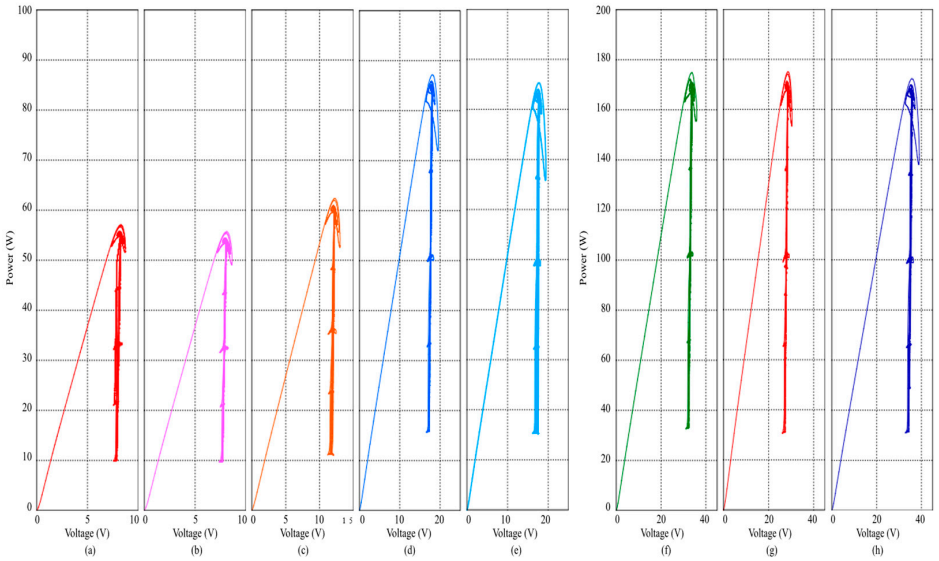

Figure 26. MPP trajectories of mixed-connection PV generation system based on proposed scheme: (**a**) PV_{11}, (**b**) PV_{12}, (**c**) PV_{13}, (**d**) PV_{21}, (**e**) PV_{22}, (**f**) PV_{31}, (**g**) PV $String_1$, and (**h**) PV $String_2$.

Figure 27 shows the trajectories of the maximum power points of each PV module or PV module string in the mixed-connection PV generation system using the EPO algorithm. Except for the maximum power point of PV_{12}, which fluctuates slightly, as its received irradiance remains constant during non-uniform irradiation conditions, the maximum power point trajectories of the other PV modules or PV module strings exhibit severe oscillations. This is due to the variation in the global maximum power point of the PV generation system under varying conditions and the continuous adjustment of the system's operating voltage by the EPO algorithm, leading to the continuous variation in the maximum operating voltage of each PV module.

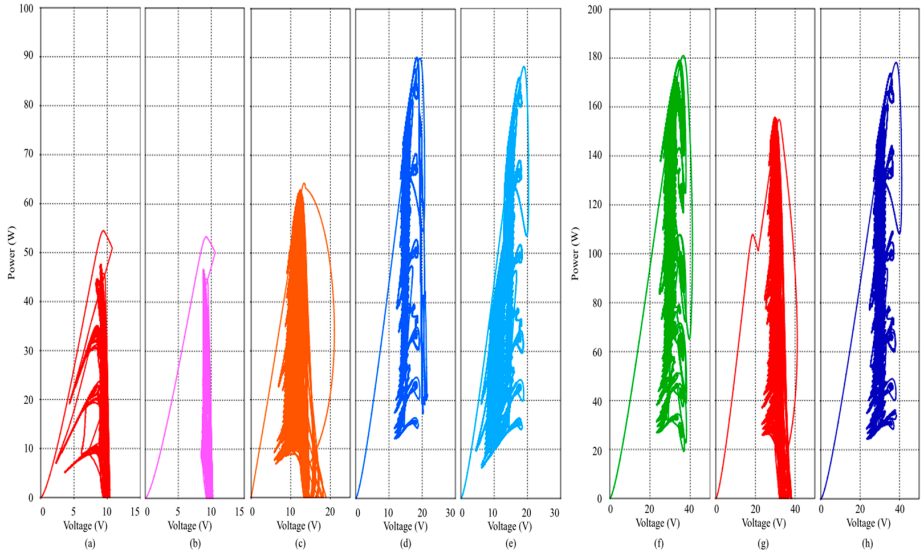

Figure 27. MPP trajectories of mixed-connection PV generation system based on EPO algorithm: (**a**) PV_{11}, (**b**) PV_{12}, (**c**) PV_{13}, (**d**) PV_{21}, (**e**) PV_{22}, (**f**) PV_{31}, (**g**) PV $String_1$, and (**h**) PV $String_2$.

5.5. Simulation Data Processing

The data retrieved from the 'To File' block are utilized for computing various parameters in the PV generation system. These parameters encompass the mean real maximum power P_{RM}, the mean maximum power P_{SM} obtained through the proposed scheme, the mean charging power P_{CH} to the battery, the mean global maximum power P_{GM}, and the mean maximum power P_{EPO} based on the EPO algorithm. Subsequently, the maximum power tracking efficiency η_T of the proposed scheme, the overall efficiency η_S of the system, the ideal GMPPT efficiency η_G, and the tracking efficiency η_E of the EPO-based algorithm are determined and presented in Table 8.

Table 8. Mean power and scheme efficiencies.

Power (W)					Efficiency (%)			
P_{RM}	P_{SM}	P_{CH}	P_{GM}	P_{EPO}	η_T	η_S	η_G	η_E
342.74	339.84	327.11	289.42	277.65	99.15	95.44	84.44	81.01

The data presented in Table 8 disclose that the average MPPT efficiency η_T of the proposed scheme is 99.15%, the average overall efficiency η_S of the system is determined to be 95.44%, and under ideal conditions, the average efficiency η_G of the GMPPT scheme is 84.44%, while the average efficiency η_E based on the EPO algorithm is only 81.01%.

6. Discussion of Simulation Results

The simulated waveforms and data results illustrate the efficacy of the proposed solution. Whether the PV modules in the PV generation system are of the same type or different types, and whether they are connected in series, parallel, or a combination of both, as well as whether the PV generation system is under uniform or non-uniform irradiance and other complex environmental conditions, the appropriate solution put forth in this paper can address various mismatch problems encountered in practical applications.

The proposed solution initially utilizes current-equalization technology or voltage-matching methods to address mismatches caused by variations in PV module parameters and operating conditions (e.g., temperature fluctuations, aging effects, and exceeding the system's lifespan) to ensure that each PV module in the PV generation system produces adequate output power. Simultaneously, it transforms the output characteristics of the PV generation system under complex conditions from multi-peak characteristics to single-peak characteristics to enable the application of the extremum-seeking control to track the real maximum power of the PV generation system and achieve optimal overall efficiency. Hence, it is simpler, easier to implement, and more efficient than the traditional MPPT algorithm. However, the GMPPT scheme only tracks the global maximum power point of the PV generation system. Based on the analysis and simulation of the maximum power point principle described above, it is evident that the global maximum power is not the maximum value of the actual generated power of the PV generation system, and the voltage at the global maximum power point changes with environmental factors. The output characteristics of the PV generation system exhibit time-varying multi-peak characteristics, leading to significant oscillations in the tracked power.

The single-switch multi-winding forward–flyback converter effectively addresses the current mismatch in series-connected PV modules and stabilizes operating voltage. The multi-switch multi-winding forward–flyback converter achieves voltage matching for parallel connection of PV modules or module strings, enabling each PV module to operate at its maximum power point. The single-switch multi-transformer forward–flyback converter achieves both current equalization for series-connected PV modules and voltage matching among PV modules or PV module strings. Each type of converter can operate independently or be connected in series or parallel to accommodate the requirements of PV generation systems with different voltage or power levels, subject to the electrical safety for practical applications and the consideration of overcharge protection of the storage battery.

The improved extremum-seeking control used in this paper only introduces disturbances to the PV generation system's operating voltage. By detecting the disturbance amount in the system's power and current, the direction of the perturbation voltage can be determined, and the magnitude can be adjusted according to the varying irradiance, improving the tracking speed and eliminating power oscillation without requiring extensive knowledge about the system, making it convenient for system designers to apply. Furthermore, this control method can be implemented using analog circuits or digital methods, making it suitable for personnel from different technical backgrounds.

This paper presents a solution to address the mismatch issue in PV generation systems that consist of diverse PV modules, using the charging of RV storage batteries as an illustration. While this specific case may not be widely encountered in practical applications, the problem of mismatch in PV generation systems with mixed connections of the same type of PV modules under non-uniform illumination conditions is quite common, as mentioned in the last paragraph of Section 2.2. Consequently, the solution proposed in this paper is also applicable to PV generation systems with the same type of PV modules.

7. Conclusions

This paper briefly reviews the development trends and existing issues of PV generation technology in the context of RV electrical energy supplementation. It evaluates the merits and demerits of existing schemes (e.g., GMPPT algorithms, DMPPT methods, and DPP techniques) in achieving optimal power for multi-type mixed-connection PV systems. By considering the distinctive output characteristics of PV modules with different configurations (series, parallel, and mixed connections), it summarizes the configuration methods of PV modules for mixed-connection PV generation systems applied to RV power supplementation. Building on this foundation, a novel equalization solution based on extremum-seeking control is introduced and assessed using the PLECS simulation platform. The simulation results demonstrate a substantial enhancement in the output efficiency of PV modules, leading to an impressive system efficiency of 95.44%, marking a substantial 14.43% improvement over GMPPT schemes utilizing the EPO algorithm. The innovation of the proposed solution is distinguished by three key aspects. Firstly, the equalization circuit based on a forward–flyback converter achieves current equalization among series PV modules or voltage matching between parallel PV module strings during power transfer, eliminating the necessity for current or voltage detection. This feature streamlines circuit design, thereby reducing system costs. Secondly, the equalization circuit simplifies the multi-peak characteristic of the output power of the PV generation system into a single-peak characteristic. This transformation facilitates real-time attainment of the maximum output power through ESC without mandating extensive system expertise. Lastly, the improved ESC enhances the system's responsiveness to environmental fluctuations, thereby optimizing its operational efficiency. This innovative solution addresses a crucial gap in power optimization research concerning multi-type, mixed-connection PV generation systems and serves as a valuable resource for design engineers and researchers involved in the development of PV generation systems.

Author Contributions: Conceptualization, methodology, validation, and writing, D.T.; review and editing, D.T., F.L.S. and T.H.G.T. All authors have read and agreed to the published version of the manuscript.

Funding: This research received no external funding.

Data Availability Statement: The original contributions presented in the study are included in the article, further inquiries can be directed to the corresponding author.

Acknowledgments: DaiBin Tang gratefully thanks Plexim GmbH, Switzerland, for providing the electrical engineering software PLECS as an academic sponsorship for this research.

Conflicts of Interest: The authors declare no conflicts of interest.

References

1. Wang, E.; De Bono, A.; Wong, I. A Case Study: Designing a Sustainable Recreational Vehicle for the Emerging Market through Computer-Aided Design Process. *Comput. Aided Des. Appl.* **2014**, *11*, S27–S35. [CrossRef]
2. Belhachat, F.; Larbes, C. Comprehensive Review on Global Maximum Power Point Tracking Techniques for PV Systems Subjected to Partial Shading Conditions. *Sol. Energy* **2019**, *183*, 476–500. [CrossRef]
3. Yamaguchi, M.; Masuda, T.; Araki, K.; Sato, D.; Lee, K.; Kojima, N.; Takamoto, T.; Okumura, K.; Satou, A.; Yamada, K.; et al. Development of High-efficiency and Low-cost Solar Cells for PV-powered Vehicles Application. *Prog. Photovolt.* **2021**, *29*, 684–693. [CrossRef]
4. Mohammad, A.; Zamora, R.; Lie, T.T. Integration of Electric Vehicles in the Distribution Network: A Review of PV Based Electric Vehicle Modelling. *Energies* **2020**, *13*, 4541. [CrossRef]
5. Häberlin, H. *Photovoltaics: System Design and Practice*, 1st ed.; Wiley: Hoboken, NJ, USA, 2012; ISBN 978-1-119-99285-1.
6. Chu, G.; Wen, H.; Yang, Y.; Wang, Y. Elimination of Photovoltaic Mismatching With Improved Submodule Differential Power Processing. *IEEE Trans. Ind. Electron.* **2020**, *67*, 2822–2833. [CrossRef]
7. Nadeem, A.; Hussain, A. A Comprehensive Review of Global Maximum Power Point Tracking Algorithms for Photovoltaic Systems. *Energy Syst.* **2023**, *14*, 293–334. [CrossRef]
8. Yuan, J.; Zhao, Z.; Liu, Y.; He, B.; Wang, L.; Xie, B.; Gao, Y. DMPPT Control of Photovoltaic Microgrid Based on Improved Sparrow Search Algorithm. *IEEE Access* **2021**, *9*, 16623–16629. [CrossRef]
9. Wang, F.; Zhu, T.; Zhuo, F.; Yang, Y. Analysis and Comparison of FPP and DPP Structure Based DMPPT PV System. In Proceedings of the 2016 IEEE 8th International Power Electronics and Motion Control Conference (IPEMC-ECCE Asia), Hefei, China, 22–26 May 2016; IEEE: Piscataway, NJ, USA, 2016; pp. 207–211.
10. Jeong, H.; Lee, H.; Liu, Y.-C.; Kim, K.A. Review of Differential Power Processing Converter Techniques for Photovoltaic Applications. *IEEE Trans. Energy Convers.* **2019**, *34*, 351–360. [CrossRef]
11. Jeon, Y.-T.; Lee, H.; Kim, K.A.; Park, J.-H. Least Power Point Tracking Method for Photovoltaic Differential Power Processing Systems. *IEEE Trans. Power Electron.* **2017**, *32*, 1941–1951. [CrossRef]
12. Shenoy, P.S.; Kim, K.A.; Krein, P.T. Comparative Analysis of Differential Power Conversion Architectures and Controls for Solar Photovoltaics. In Proceedings of the 2012 IEEE 13th Workshop on Control and Modeling for Power Electronics (COMPEL), Kyoto, Japan, 10–13 June 2012; IEEE: Piscataway, NJ, USA, 2012; pp. 1–7.
13. Chu, G.; Wen, H.; Ye, Z.; Li, X. Design and Optimization of the PV-Virtual-Bus Differential Power Processing Photovoltaic Systems. In Proceedings of the 2017 IEEE 6th International Conference on Renewable Energy Research and Applications (ICRERA), San Diego, CA, USA, 5–8 November 2017; IEEE: Piscataway, NJ, USA, 2017; pp. 674–679.
14. Chu, G.; Wen, H.; Jiang, L.; Hu, Y.; Li, X. Bidirectional Flyback Based Isolated-Port Submodule Differential Power Processing Optimizer for Photovoltaic Applications. *Sol. Energy* **2017**, *158*, 929–940. [CrossRef]
15. Shi, F.; Song, D. A Novel High-Efficiency Double-Input Bidirectional DC/DC Converter for Battery Cell-Voltage Equalizer with Flyback Transformer. *Electronics* **2019**, *8*, 1426. [CrossRef]
16. Shahid, H.; Kamran, M.; Mehmood, Z.; Saleem, M.Y.; Mudassar, M.; Haider, K. Implementation of the Novel Temperature Controller and Incremental Conductance MPPT Algorithm for Indoor Photovoltaic System. *Sol. Energy* **2018**, *163*, 235–242. [CrossRef]
17. Martinez Lopez, V.; Žindžiūtė, U.; Ziar, H.; Zeman, M.; Isabella, O. Study on the Effect of Irradiance Variability on the Efficiency of the Perturb-and-Observe Maximum Power Point Tracking Algorithm. *Energies* **2022**, *15*, 7562. [CrossRef]
18. Alik, R.; Jusoh, A. An Enhanced P&O Checking Algorithm MPPT for High Tracking Efficiency of Partially Shaded PV Module. *Sol. Energy* **2018**, *163*, 570–580. [CrossRef]
19. Tsobze, S.K.; Njomo, A.F.T.; Naoussi, S.R.D.; Kenne, G. A New Modified ESC Algorithm for MPPT Applied to a Photovoltaic System for Power Losses Mitigation under Varying Environmental Conditions. *Int. J. Dynam. Control* **2023**, *11*, 354–369. [CrossRef]
20. Tan, Y.; Nešić, D.; Mareels, I. On Non-Local Stability Properties of Extremum Seeking Control. *Automatica* **2006**, *42*, 889–903. [CrossRef]
21. Ghods, N.; Krstic, M. Source Seeking with Very Slow or Drifting Sensors. *J. Dyn. Syst. Meas. Control* **2011**, *133*, 044504. [CrossRef]
22. Krstic, M.; Ghaffari, A.; Seshagiri, S. Extremum Seeking for Wind and Solar Energy Applications. *Mech. Eng.* **2014**, *136*, S13–S21.
23. Leyva, R.; Olalla, C.; Zazo, H.; Cabal, C.; Cid-Pastor, A.; Queinnec, I.; Alonso, C. MPPT Based on Sinusoidal Extremum-Seeking Control in PV Generation. *Int. J. Photoenergy* **2012**, *2012*, 672765. [CrossRef]
24. Bizon, N. Global Maximum Power Point Tracking Based on New Extremum Seeking Control Scheme. *Prog. Photovolt. Res. Appl.* **2016**, *24*, 600–622. [CrossRef]
25. Stornelli, V.; Muttillo, M.; De Rubeis; Nardi, I. A New Simplified Five-Parameter Estimation Method for Single-Diode Model of Photovoltaic Panels. *Energies* **2019**, *12*, 4271. [CrossRef]
26. Kottas, T.L.; Boutalis, Y.S.; Karlis, A.D. New Maximum Power Point Tracker for PV Arrays Using Fuzzy Controller in Close Cooperation With Fuzzy Cognitive Networks. *IEEE Trans. Energy Convers.* **2006**, *21*, 793–803. [CrossRef]
27. Ding, K.; Zhang, J.; Bian, X.; Xu, J. A Simplified Model for Photovoltaic Modules Based on Improved Translation Equations. *Sol. Energy* **2014**, *101*, 40–52. [CrossRef]
28. Belhachat, F.; Larbes, C. Survey and Classification of Hybrid GMPPT Techniques for Photovoltaic System under Partial Shading Conditions. *ENP Eng. Sci. J.* **2022**, *2*, 31–46. [CrossRef]

29. Vijayalekshmy, S.; Rama Iyer, S.; Beevi, B. Comparative Analysis on the Performance of a Short String of Series-Connected and Parallel-Connected Photovoltaic Array Under Partial Shading. *J. Inst. Eng. India Ser. B* **2015**, *96*, 217–226. [CrossRef]
30. Velasco-Quesada, G.; Guinjoan-Gispert, F.; Pique-Lopez, R.; Roman-Lumbreras, M.; Conesa-Roca, A. Electrical PV Array Reconfiguration Strategy for Energy Extraction Improvement in Grid-Connected PV Systems. *IEEE Trans. Ind. Electron.* **2009**, *56*, 4319–4331. [CrossRef]
31. Yilmaz, M.; Krein, P.T. Review of Battery Charger Topologies, Charging Power Levels, and Infrastructure for Plug-In Electric and Hybrid Vehicles. *IEEE Trans. Power Electron.* **2013**, *28*, 2151–2169. [CrossRef]
32. Lee, J.-H.; Park, J.-H.; Jeon, J.H. Series-Connected Forward–Flyback Converter for High Step-Up Power Conversion. *IEEE Trans. Power Electron.* **2011**, *26*, 3629–3641. [CrossRef]
33. Shang, Y.; Xia, B.; Zhang, C.; Cui, N.; Yang, J.; Mi, C.C. An Automatic Equalizer Based on Forward–Flyback Converter for Series-Connected Battery Strings. *IEEE Trans. Ind. Electron.* **2017**, *64*, 5380–5391. [CrossRef]
34. Bizon, N.; Thounthong, P.; Raducu, M.; Constantinescu, L.M. Designing and Modelling of the Asymptotic Perturbed Extremum Seeking Control Scheme for Tracking the Global Extreme. *Int. J. Hydrogen Energy* **2017**, *42*, 17632–17644. [CrossRef]
35. Luo, H.; Wen, H.; Li, X.; Jiang, L.; Hu, Y. Synchronous Buck Converter Based Low-Cost and High-Efficiency Sub-Module DMPPT PV System under Partial Shading Conditions. *Energy Convers. Manag.* **2016**, *126*, 473–487. [CrossRef]
36. Liu, Z.; Ma, J.; Liu, K. Research on Control Method of Neutral Point Potential Balance of T-Type Three-Level Inverter Based on PLECS. *J. Phys. Conf. Ser.* **2021**, *2087*, 012051. [CrossRef]
37. Akpolat, A.N.; Yang, Y.; Blaabjerg, F.; Dursun, E.; Kuzucuoglu, A.E. Modeling Photovoltaic String in PLECS Under Partial Shading. In Proceedings of the 2019 International Conference on Power Generation Systems and Renewable Energy Technologies (PGSRET), Istanbul, Turkey, 26–27 August 2019; IEEE: Piscataway, NJ, USA, 2019; pp. 1–6.
38. Allmeling, J.; Hammer, W. PLECS User Manual. Available online: https://www.plexim.com/ (accessed on 9 September 2023).